Nanoscale Research Letters

NANO EXPRESS Open Access

Novel Chemo-Photothermal Therapy in Breast Cancer Using Methotrexate-Loaded Folic Acid Conjugated Au@SiO_2 Nanoparticles

Reza Agabeigi[1], Seyed Hossein Rasta[2], Mohammad Rahmati-Yamchi[1], Roya Salehi[3*] and Effat Alizadeh[1*]

Abstract

Low level laser therapy (LLLT) is known as a safe type of phototherapy to target tumor tissue/cells. Besides, using targeted nanoparticles increases the successfulness of cancer therapy. This study was designed for investigating the combined effect of folate (FA)/Methotrexate (MTX) loaded silica coated gold (Au@SiO_2) nanoparticles (NPs) and LLLT on the fight against breast cancer.

NPs were synthesized and characterized using FTIR, TEM and DLS-Zeta. The NPs had spherical morphology with mean diameter of around 25 nm and positive charge (+13.3 mV) while after conjugation with FA and MTX their net charge reduced to around -19.7 mV.

Our findings in cell uptake studies clearly showed enhanced cellular uptake of NPs after FA and MTX loaded NPs in both breast cancer cell lines especially on MDA-MB-231 due to high expression of folate receptors. The results indicated that LLLT had a proliferative effect on both breast cancer cell lines but in the presence of engineered breast cancer targeted nanoparticle, the efficacy of combination chemo-photothermal therapy was significantly increased using MTT assay ($p<0.05$), DAPI staining, and cell cycle findings. The highest apoptotic effect on breast cancer cell lines was observed in the cells exposed to a combination of MTX-FA loaded Au@SiO_2 NP and LLLT proved by DAPI staining and cell cycle(by increasing the cell arrest in subG0/G1). Taken together a combination of chemotherapy and LLLT improves the potential of breast cancer therapy with minimum side effects.

Keywords: Au@SiO_2 nanoparticles, Low level laser therapy, Methotrexate, Folic acid, Breast cancer

Introduction

Breast cancer (BC), as the most frequent women, affecting cancer recently has reported with 1.7 million new cases worldwide [1]. Because of its complicated etiology and poor response to the treatment, often known to be the central cause of cancer associated deaths of women universally [2–5]. About 40,000 women in the U.S. were predictable to die from BC in 2014 [2, 6, 7] "(www.cancer.org)". With the 522,000 deaths overall, it is the fifth cause of death from cancer with around 800,000 cases in less developed and about the same frequency in developed regions [1]. In Asian countries the greatest age of beginning is among adults of 40 or 50 years in comparison with the western countries which is frequent among 60–70 years [8]. The major risk factors of BC are female sex, family history, age, and varying generative leanings, such as first childbirth at the age of more than 30 years, early menarche and later menopause, and nulliparity [9].

The main aim in the fight against cancer is developing effective therapeutic plans with low toxicities and high

* Correspondence: salehiro@tbzmed.ac.ir; alizadehe@tbzmed.ac.ir
[3]Drug Applied Research Center and Department of Medical Nanotechnology, Faculty of Advanced Medical Sciences, Tabriz University of Medical Sciences, Tabriz, Iran
[1]Department of Medical Biotechnology, Faculty of Advanced Medical Sciences, Tabriz University of Medical Sciences, Tabriz, Iran
Full list of author information is available at the end of the article

specificities to eliminate tumors, mainly their metastases, and further their recurrence prevention. But presently used cancer treatment approaches, such as surgery, chemotherapy and radiotherapy showed various side effects [10–12] and all fail to achieve this aim [13, 14]

The past few decades have observed major struggles in the treatment of cancer [15, 16]. Between the current popular therapeutic approaches, thermal therapy has grown as a prospective treatment method [17]. Recently photothermal therapy (PTT), as a potentially effective and non-invasive cancer therapy, has attracted significant attention [18, 19]. PTT based on photo-absorbing nanostructures has become a different way to the general methods [20, 21]. In a typical PTT, that use PTT agents to destroy tumor by getting enough hyperthermia (42°C) under laser irradiation (near-infrared (NIR) light in the range of 700–1100 nm), has been studied as a greatly precise and negligibly invasive method of cancer treatment [22–28].

A number of nanoparticles have been widely studied as imaging contrast agents, drug delivery carrier, and transformer of energy modalities such as laser, radiowaves, and ultrasound, to thermal phenomena responsible for therapeutic effects [29–39].

Gold nanoparticles have attracted great attention during the past decade due to their high localized surface plasmon resonance (LSPR) and easy surface conjugation with biomolecules [40]. They have revealed high-performance photothermal conversion capacity in the NIR area [41–43] without harmful side effects in biological systems [44].

Although gold nanoparticles have been recognized as a promising photo-synthesizer, but due to their poor photothermal stability upon repetitive NIR irradiation, gold nanoparticles gradually lose their photothermal converting ability that limited their use in clinical practice. In addition, gold nanoparticles are not good drug carriers either because of their poor drug loading capacity and controlled drug release profile [45, 46]. Alternatively, mesoporous silica nanoparticle (MSN) was known to be appropriate drug, DNA and protein carrier because of its higher drug loading capability and lack of toxic contents that produced from its degradations. They also have a big surface area, controllable size, highly available pore volume, and desired surface features apply for a modification [47].

Nanoparticles after conjugating to a chemotherapeutic agent and cancer targeting ligand can inhibit disadvantages of routine chemotherapy, such as un-specific delivery, poor water solubility, and low therapeutic indices [48, 49].

Agents showing chemotherapeutic properties such as doxorubicin, cyclophosphamide, methotrexate, fluorouracil, and docetaxel are used single-handedly or in combination as the main core treatments, or aided with other treatments like PTT. Most of cancer patients experiencing adverse effects of chemotherapy drugs due to their non-precise distribution in patient's body that affects all the organs. These drugs hurt some of the fast growing normal cells, for example blood cells, mucous membrane cells covering the internal organs, and hair follicles [50–53].

Methotrexate (MTX) has been the most frequently used drugs for rheumatoid arthritis and several types of tumors such as skin, lung, head and neck, and breast [54, 55]. It inhibits dihydrofolate reductase (DHFR), the enzyme contributing to the production of tetrahydrofolate and its byproducts which are necessary for thymidylate and purine synthesis and both of them are vital for cell growth and cell proliferation. Hence, blocking DHFR methotrexate prevents the synthesis of 4 basic macromolecules DNA, RNA, thymidylates, and proteins [56].

Unfortunately, alike to most conventional PTT agents, the main challenge is to attain selective accumulation of GNPs in the target tissue after systemic injection [57–59]. Targeted cancer therapy allows the delivery of chemotherapeutic drug to specific cancer cells while decreasing the exposure of normal healthy cells. This led us to deliver greater dosage of drug to cancer cells with lower systemic toxicity. Ligand targeted nanoparticles are precisely identified cancer cell markers, that are highly expressed on the cancer cell surface [40].

Folic acid (folate or vitamin B9) is a key material for cell growth and metabolism. Because of the great affinity of folate for the folate receptor proteins, it is utilized as an element for cancer targeting. Folate receptor, as a tumor biomarker, is overexpressed in definite malignant cells like breast, ovarian, lung, kidney, brain, and colon cancer [60]. Folate conjugated drug delivery systems enhance cellular uptake of drug via endocytosis [61].

Materials and Method

Reagents and materials

We used double distilled water (Ghazi Company, Tabriz, Iran) and analytical grade chemical reagents for our experiments. A number of reagents were purchased from Sigma-Aldrich Company including: Tetraethyl orthosilicate (TEOS, 98%), (3-Mercaptopropyl) trimethoxysilane (MPTES,95% purity), folic acid and rhodamine B. A group of materials was purchased from Merck Co: Hydrochloric Acid (HCl, 37%), Ammonia solution (25%), toluene Sodium hydroxide (NaOH, 98%), and further solvents. MTX was bought from Zahravi Farma Company, Tabriz, Iran.

Instrumentation

In this study, for analyzing the particles size and morphology, transmission electron microscopy (TEM) (LEO

906, Germany) was employed. We prepared around 100μL of our nanoparticles suspended in aqueous solution at room temperatures. The solution was transferred onto a carbon film coated on a copper grid of TEM with subsequent freeze drying and observed at 80KV. Determination of particle size was performed by DLS (dynamic light scattering) measurement at 25 °C using a Zetasizer Nano ZS90, Malvern Instruments, Malvern, UK. The Zeta potential measurements for the prepared NPs were performed by photon correlation spectroscopy (Zetasizer-ZS, Malvern Instrument, UK). A double beam UV–Vis spectrophotometer (UV-1601 PC model SHIMADZU, Kyoto, Japan) was employed for absorbance measuring by 700μL quartz cuvette having 10 mm path length. Fourier transforms infrared (FTIR) spectroscopy from Bruker Tensor 27 spectrometer, Germany was utilized for KBr pellet method performing. The pH measurements were done with a Metrohm 713 pH-meter (Herisau, Switzerland). The mechanical stirrer Heidolph RZR 2102 Control Overhead Stirrer (Schwabach, Germany) was used for stirrings. The encapsulation efficiency of FA and MTX was calculated using the HPLC system consisted of Waters 2690 separation module equipped with a UV–vis detector Waters 2500 Pump 1000 detectors (Waters, Milford, MA). The chromatographic separation was implemented at ambient temperature using a C18 m Bondapak (250 mm 4.6 mm, 10 mm, 125 A Waters, Ireland) chromatography columns.

Preparation of Au@SiO_2 Nanoparticles

The SiO_2 NPs were synthesized based on the sol–gel method reported previously [62, 63]. In the next step thiol-functionalized silica-coated nanoparticles (TFSNPs) were prepared according to the method mentioned in our previous study [64]. The Au nanoparticles were produced by a citrate reduction method (Turkevich method) [65]. Finally, the surface of TFSNPs was covered by AuNPs. At first TFSNPs were dispersed in water with the aid of the bath sonicator for at least one hour and added to the AuNPs solution and sonicated for additional 30 min. The reaction was done at dark condition for two days in dynamic stirring at 25 °C. The Au@SiO_2 nanoparticles with purple colored appearance were collected by centrifugation (10000 rpm, 10 min) and dried in a vacuum oven.

MTX and FA loading

MTX as well as FA were loaded into the Au@SiO_2 nanocarrier as follows: MTX (10 mg) was added to a 10 mL well-dispersed suspension of nanocarrier in PBS (5 mg/mL, pH 7.4) and agitated moderately at room temperature for one day in dark conditions. The MTX loaded Au@SiO_2 nanocarrier was collected by centrifugation. The supernatant was collected for the measurement of unloaded MTX. Then MTX loaded Au@SiO_2 nanocarrier was dispersed in PBS (5 mg/ mL, pH 7.4) and FA (10mg) were added to the solution and stirred moderately at room temperature for another day in dark conditions. The FA-MTX loaded Au@SiO_2 nanocarrier was gathered by centrifugation and the supernatant was separated for the calculation of unbound FA in the final step. The FA-MTX loaded Au@SiO_2 nanocarrier was freeze-dried and stored for next experiments. The amounts of unbound MTX and FA were calculated using HPLC method by protocol reported previously [66]. Folic acid was dissolved in ammonium hydroxide (10 wt %) and diluted with the mobile phase. The retention time for MTX and Folic acid were 10.5 and 5.95 min, respectively. Triplicate samples were applied. The drug loading efficiency (DLE) was calculated by the following formulas:

$$ee(\%) = \frac{(initial\ total\ drugs - Unabsorbed\ drugs)}{Initial\ total\ drugs} \times 100 \quad (1)$$

Cell lines selection and culture

Two breast cancer cell lines of interest with reported surface expression levels folate receptor (FR) [67] including MCF-7 and MDA-MB-231 was selected and purchased from the Pasteur Cell Bank (Tehran, Iran) for the cytotoxicity investigations. The selected cell lines were grown in complete medium containing RPMI1640 (Thermoscientific), 10% Fetal bovine serum (FBS), and

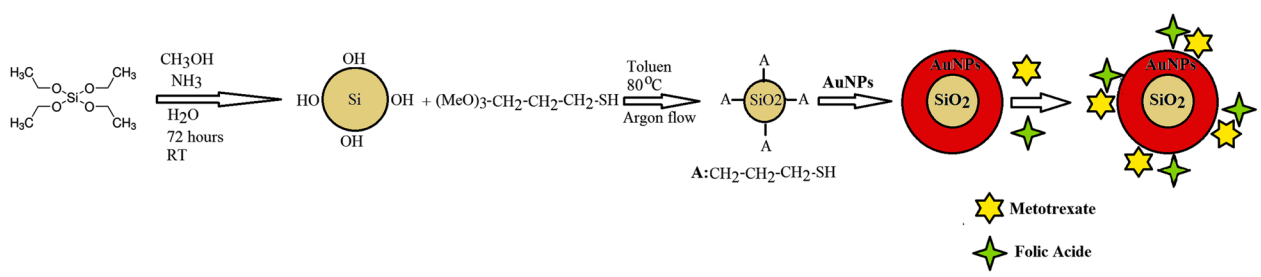

Fig. 1 The stepwise synthetic scheme for the preparation of folate and methotrexate loaded biocompatible Au@SiO_2 NPs nanoparticles

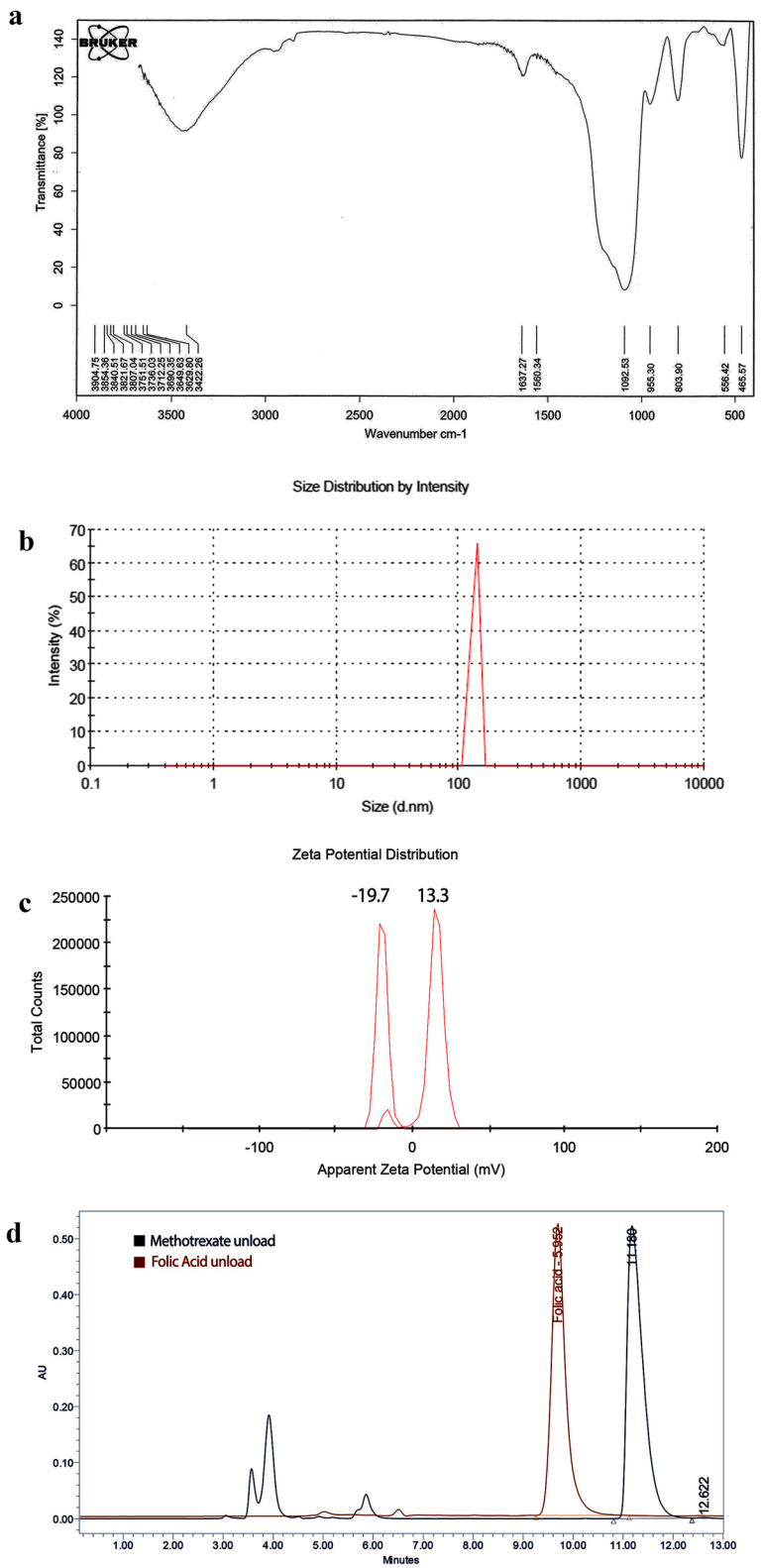

Fig. 2 **a**) FTIR spectra of Au@SiO_2 nanoparticles, **b**) size distribution of FA-MTX conjugated Au@SiO_2 NPs measured by dynamic light scattering (DLS) **c**) The zeta potential of Au@SiO_2 and FA-MTX conjugated Au@SiO_2 NPs measured by dynamic light scattering (DLS) at pH=7.4 and T=25 °C, **d**) Chromatogram of unloaded MTX and FA separated from FA-MTX conjugated Au@SiO_2 NP measured simultaneously by HPLC method

1% Penstrep (Thermoscientific) in thermal and atmospheric conditions of 37°C, 5% CO_2, and 95% humidity.

Cell cytotoxicity assay

Cell viability assays were performed for measuring cell proliferation after different NPs treatments without laser irradiation. Briefly: the MCF-7 or MDA-MB-231 cells were plated in 96 microplates with cell density of 1.5×10^4 for 24 h, then cells were treated with MTX, Au@SiO_2 and FA-MTX loaded Au@SiO_2 NPs. The cells without treatment were considered as control. At the next step, the tetrazolium dye MTT (Sigma) at final concentrations of 5 μg/ml was added to the cells and incubated at 37°C for 4 h. Then, the MTT solution was removed and the settled Furmazan crystals were dissolved in Dimethyl Sulfoxide (DMSO) (BioIdea, Iran) under gentle shaking for 10 min. Finally, the absorbance was measured in 570 nm by an ELISA reader. The viability of cells was normalized to control cells and background was removed by subtraction of blank measurements.

In vitro laser therapy

For Low Level Laser Therapy (LLLT), 810 nm wavelength NIR laser (Diode laser Mustang 2000, Russia) with 185 mW output power dose was used for cancer cell destruction. At first MCF-7 and MDA-MB 231 cells with cell density of 1.5×10^4 treated with the Au@SiO_2 and FA-MTX loaded Au@SiO_2 NPs then were exposed to laser irradiation with different laser doses (30, 60, 75, 90 and 105 J/cm^2) and fixed exposure time (139 sec). The cells exposed to only laser irradiation (without NPs) and the cells without any NPs and laser treatments considered as positive and negative control, respectively. After 24 h of laser irradiation the cell viability was measured by MTT assay method [64].

Nanoparticles cellular uptake assay

A detailed checking of the NPs cell internalization is essential in order to confirm the specific effect of surface modified nanocarrier for each cell line. In the present work, we employed both flow cytometry as quantitative and fluorescence microscopy for qualitative checking the up-take of NPs by MCF-7 and MDA-MB-231 cell lines.

For suspension of NPs, the rhodamine B (RhoD) solution in PBS was added along with stirring for 24 h at ambient temperature and dark room (preventing bleaching). Then, RhoD-loaded NPs were separated by Amicon Filter with nominal molecular weight limit (NMWL) of 30 kDa and centrifuged for 15 min at 5000 rpm and washed with PBS buffer to eliminate the unbounded RhoD. The cells were seeded in plates at the density of 5×10^5 per well and let to reach confluence. The cells were treated with Rhodamin B-loaded NPs for 30, 90 and 180 minutes, non-treated cells used as control. Afterwards, the cells were trypsinized and washed with PBS, and then fluorescence was quantified with flow cytometric analysis (BD Biosciences FCASCalibur flow cytometer; BD Biosciences, San Jose, CA, USA). The

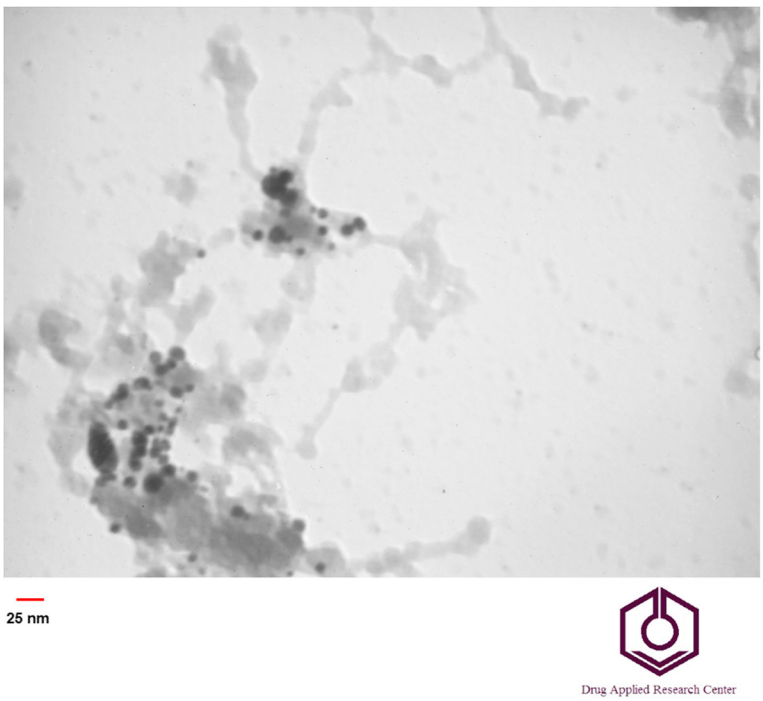

Fig. 3 TEM image of Au@SiO_2 nanoparticles

Intracellular uptake of rhodamine B-labeled NP or NPD was further confirmed by fluorescence microscopy. MCF-7 and MDA-MB-231 cells were grown on coverslips and after 24 h cells were treated with free Au@SiO_2 NPs and MTX-FA loaded Au@SiO_2 NPs. After incubation for 30, 90 and 180 minutes, the cells were washed with PBS and rhodamine B labelled nanocarrier uptakes was observed using a fluorescence microscope (Olympus microscope Bh2- FCA, Japan).

Apoptosis study by Fluorescence microscopy

One method for the nuclear qualitative study of apoptosis is a fluorescent dye DAPI which binds to DNA and is detectable by appropriate microscopic. We used a protocol as previously reported for DAPI staining [68], shortly: the MCF-7 or MDA-MB-231 cells were plated in 6 well format vessels at a density of 5 $\times 10^5$ and let them attach and grow for 24 hours. After treatment with MTX, Au@SiO_2 NPs and MTX-FA loaded Au@SiO_2 NPs with and without laser treatment the cells were washed with PBS (Sigma) and then subjected to fixation by 10% formaldehyde (Merck), next: cells were permeabilized with Triton X-100 (Sigma) for 15 minutes. After proper washings, the cells were stained with DAPI (sigma) for 5 min. Finally, the apoptotic nuclei (fragmented or wrinkled) were visualized by a Fluorescence microscope (Olympus). The cells without any treatment were considered as negative control and the cells received only laser irradiation as positive control.

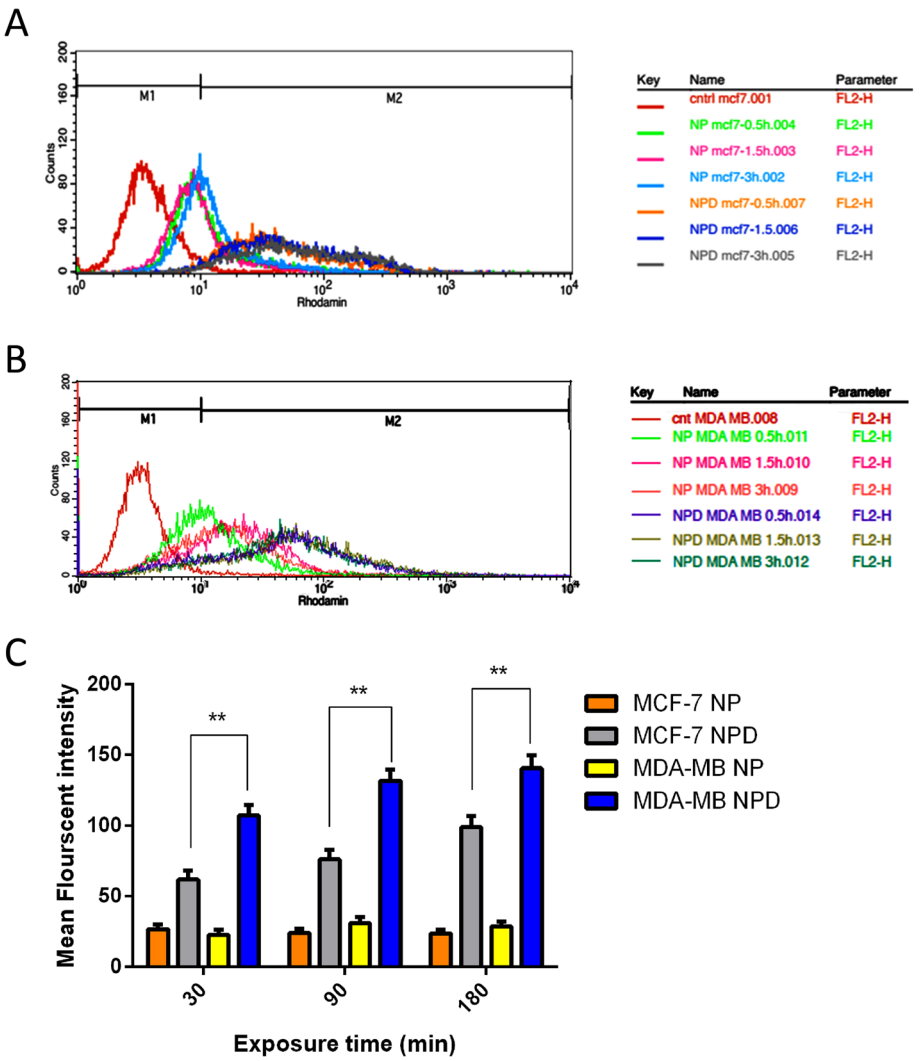

Fig. 4 Quantitative cell uptake assay of rhodamine B-labelled Au@SiO_2 nanoparticles (NP) or rhodamine B-labelled MTX-FA loaded Au@SiO_2 nanoparticles (NPD) in MCF-7 (**a**) and MDA-MB-231(**b**) cell lines for exposure durations of 0.5 h, 1.5 h and 3h obtained by flow cytometry. Non-treated cells of both cell lines were employed as negative control. **c** Comparison of mean fluorescent intensity of rhodamine B-labelled Au@SiO_2 nanoparticles (NP) or rhodamine B-labelled MTX-FA loaded Au@SiO_2 nanoparticles (NPD) for exposure durations of 0.5 h, 1.5 h and 3h obtained by flow cytometry

Investigations of cell cycle disturbances

The MCF-7 and MDA-MB-231 cell cycle distributions were determined by flowcytometry analysis. In this way, the cells were seeded with starting populations of 5 × 10^5 and allowed to reach 80% confluence. Subsequently, the cells treated with MTX, Au@SiO_2 NPs and MTX-FA loaded Au@SiO_2 NPs with and without laser irradiation was performed. The cells without any treatment were considered as negative control and the cells received only laser irradiation as positive control. Then, the cells were harvested by trypsinization following with proper PBS washings. Next, the cells were fixed by Ethanol (Merck) for 48 hours. At the next step, the fixed cells were washed, then treated with Ribonuclease A (Cinaclone), with subsequent addition of propidium iodide (PI) (Sigma) at dark. The fluorescence signals were detected by FACS set from Beckton Dicinson Company.

Statistics of the study

The experiments for each step have been performed in three repeats and the results were reported as mean ± SD. The ANOVA was used for comparison of significance among groups. The differences were reflected significances where probability value was calculated <0.05 by SPSS software.

Results and discussion

Characterization of synthesized NPs

The Au@SiO_2 NPs was produced in four steps: 1-synthesis of SiO_2 nanoparticles, 2-addition of thiol containing linker to SiO2 NPs, 3-synthesis of gold nanoparticles, and 4-attaching the gold nanoparticles to the surface of SiO2-linker complexes (Fig. 1). The successful synthesis of Au@SiO_2 was confirmed by FTIR (Fig. 2a). The Si–O–Si peak was appeared around 1088 cm^{-1}. A

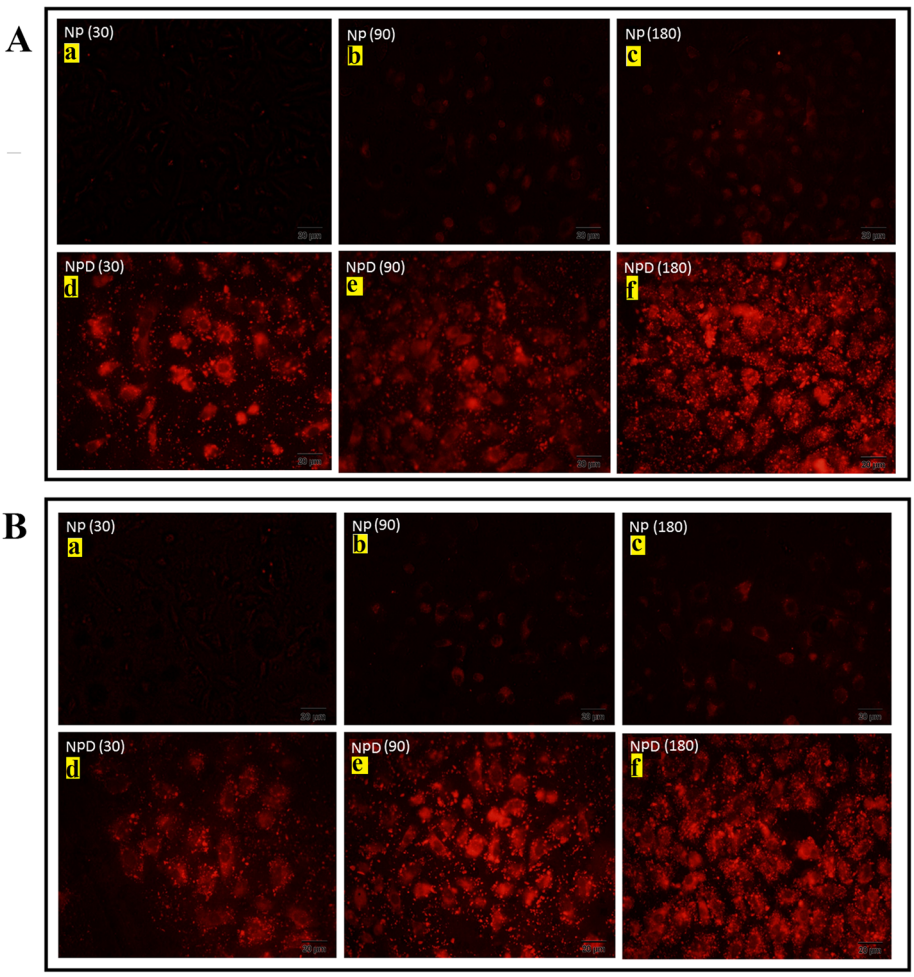

Fig. 5 A Qualitative cell uptake assay using Rhodamine B-labelled Au@SiO_2 nanoparticles (NP) in MCF7 with exposure durations of 30 (**a**), 90 (**b**) and 180 (**c**) min or rhodamine B-labelled MTX-FA loaded Au@SiO_2 nanoparticles (NPD) with exposure durations of 30 (**d**), 90 (**e**) and 180 (**f**) min and (**B**) Qualitative cell uptake assay using Rhodamine B-labelled Au@SiO_2 nanoparticles (NP) in MDA-MB-231 with exposure durations of 30 (**a**), 90 (**b**) and 180 (**c**) min or rhodamine B-labelled MTX-FA loaded Au@SiO_2 nanoparticles (NPD) with exposure durations of 30 (**d**), 90 (**e**) and 180 (**f**) min captured by florescent microscopy

wide peak at 3000–3700 and 803 cm^{-1} is credited to the stretching and out-of plane bending of free-silanol O–H groups, respectively. The aliphatic C–H stretching vibration was showed as strong peak at 2950 cm^{-1}. The C–O of three methoxy silane groups was showed by peak at 1191 cm^{-1}.

Dynamic light scattering (DLS) measurements indicated that FA-MTX conjugated Au@SiO_2 NPs size was in the nanometer range (105±2.3 nm) with narrow size distribution (Fig. 2b).

Zeta potential is an important physicochemical parameter that influences the stability of nanosuspensions. Extremely positive or negative zeta potential values cause larger repulsive forces. On the other hand, the high charge of the particles, whether positive or negative, causes the NPs to be absorbed by the phagocytes of the liver and disposed of the body. In the case of a combined electrostatic and steric stabilization, a minimum zeta potential of ± 20 mV is desirable [69–71]. The zeta potential data of NPs were compared before and after loading with the MTX-FA at pH=7.4 and T=25 °C (Fig. 2c). The obtained zeta potentials of Au@SiO_2 NPs were +13.3 mV which after dual drug loading decreased to -19.7 mV which were in the desirable range. The MTX and

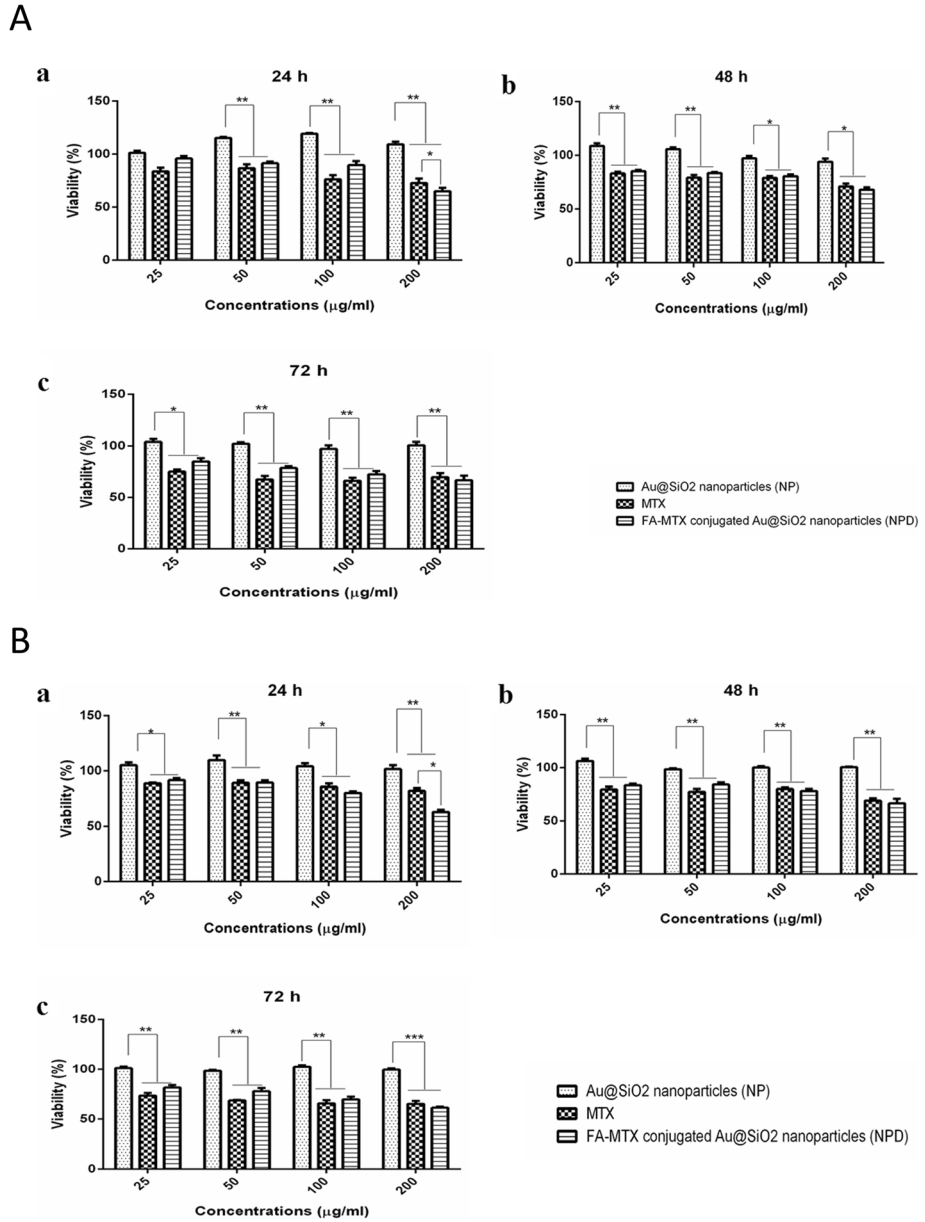

Fig. 6 a MCF-7 and (**b**) MDA-MB-231 cells growth inhibition rates after treatment with different concentration of NP, MTX and FA-MTX loaded Au@SiO_2 nanoparticles (NPD) after exposure time of 24, 48 and 72h

FA had a negative net charge at pH (7.4) above its pka (3.8 and 4.8, 3.5 and 4.3), due to the de-protonation of two carboxylic acid groups in its structure ([72], https://pubchem.ncbi.nlm.nih.gov.). Therefore, after MTX and FA simultaneous loading on Au@SiO_2 NPs, the net charge became negative.

TEM analysis provides the definite individual particle size. Au nanoparticle was seen as dark spheres dispersed on the SiO2 NPs as a gray bed layer. TEM images confirmed that the Au@SiO2 NPs have synthesized with homogenous spherical shape in which the particles average size was around 25nm (Fig. 3).

Drug loading

Herein, folate is mediating the increased uptake of GNPs in the certain types of cancer cells that overexpressed folate receptor through receptor mediated endocytosis to overwhelm the low efficacy of internalization of GNPs, therefor the folate receptor known as a tumor marker and folate use increasingly for tumor targeting [67, 73].

After MTX and FA molecules conjugation into Au@SiO_2 NPs, the zeta potential changed from +13.3 to -19.7 mV. The estimated pKa values of the two carboxylic acid moieties of MTX is 3.8, 4.8 and FA is 3.5 and 4.3 [72], https://pubchem.ncbi.nlm.nih.gov. Therefore, due to de-protonation of two carboxylic acid groups of MTX and FA at pH 7.4 which is above their pka, the net charge became negative and indicating the successful conjugation of MTX and FA on Au@SiO_2 NPs. De Ying Tian et al shows that MTX loading on Au nanoparticles by 18 and 30 mm diameter are 15 ± 0.4% and 10 ±1.0% respectively [74]. In this study FA and MTX were loaded in Au@SiO2 NPs with encapsulation efficiency of 22.6 and 77.5%, respectively. Chromatogram of simultaneous MTX and FA assessment peak has shown in Fig. 2d.

Cell uptake

Because the intracellular photothermal agents can improve the efficiency of photothermal cancer therapy [75], it has been believed that cell internalization of photothermal materials is necessary. *In vitro* cellular uptake test was performed using human breast cancer MDA-MB-231 cells, known to highly overexpress the folate receptor [40]. To study the role of FA as a targeting agent and the efficiency of the surface coating on the uptake of the Au@SiO_2 NPs by target cells, MCF-7 and MDA-

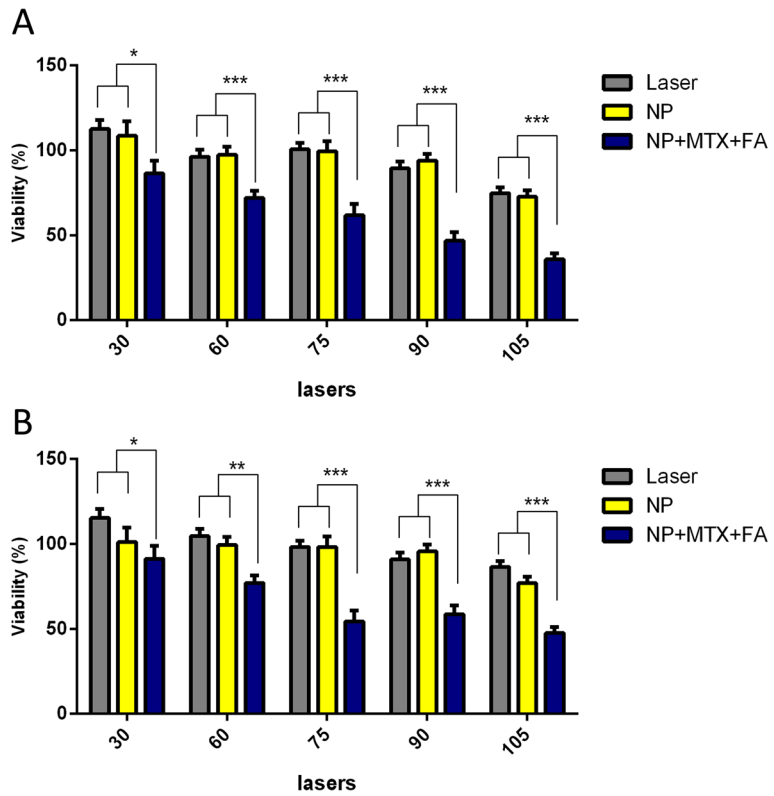

Fig. 7 A comparison of cell growth inhibition rates exposed to different laser powers (30, 60, 75, 90 and 105 J/cm^2) for treatment groups of laser alone, laser + Au@SiO2 nanoparticles and laser + MTX-FA loaded Au@SiO2 nanoparticles directed for two cell line MCF-7 (**a**) and MDA-MB-231(**b**) with subsequent checking after 24h

MB-231 cells were treated with Au@SiO2 NPs and MTX-FA loaded Au@SiO2 NPs. The mean florescent intensity results of cell uptake were shown in Fig. 4. The results showed that Au@SiO2 NPs uptake in both MCF-7 and MDA-MB-231 was increased over cell culture time for all samples (Figs. 4 and 5). Also, after surface decoration of Au@SiO2 NPs with MTX and FA, the cells uptake was increased significantly on both MCF-7 and MDA-MB-231 as folate receptor expressing cells. MTX-FA-loaded Au@SiO2 NPs uptake into MDA-MB-231 cells was greater than MCF-7. Because MDA-MB-231 cells express higher levels of surface folate receptors so high portion of folate receptor targeted NPs were entered via receptor mediated endocytosis mechanism resulting in higher cellular uptake. In another study, the increased cell internalization of the folate conjugated NPs is occurring just in the cancer cells that overexpress the aHFR and not in the healthy cells that has less cell surface express of aHFRs [40]. Conjugation of Au@SiO2 NPs with FA can facilitate the cell uptake of NPs and methotrexate, leading to boosted toxicity toward to MDA-MB-231 cells [76].

Cytotoxicity assay

In vitro cellular cytotoxicity studies of the free MTX, blank Au@SiO_2 NPs and MTX-FA conjugated Au@SiO_2 NPs, were evaluated by MTT assay for 24, 48, and 72 h (Fig. 6). The MTT assay results showed that Au@SiO_2 NPs had no cytotoxic effect on the MCF-7 and MDA-MB-231 cell lines. Furthermore, to compare the cytotoxicity effects of both free MTX and MTX-FA conjugated Au@SiO_2 NPs, the same concentration of MTX (25, 50, 100 and 200μg/mL) was used for all treatment times. Cell cytotoxicity results indicate that free MTX or MTX-FA conjugated Au@SiO_2 NPs showed around 10-25% mortality rate in both cell lines after 24h of treatment. Previous studies reported the proliferative effect of gold nanoparticles on different cell lines like murine osteoblast MC3T3-E1 cells and human periodontal ligament stem cells under in vitro conditions. Our results are in line with these studies and Figure 6a and b shown the proliferative effect of free Au@SiO2 NPs. Therefore the equal cytotoxic effect of MTX and FA-MTX loaded Au@SiO2 nanoparticles (NPD) may be due to this phenomena [77, 78].

Laser irradiation

In this study, the cell viability of MCF-7 and MDA-MB 231 cells treated with Au@SiO_2 NPs and MTX-FA loaded Au@SiO_2NPs after laser irradiation with dose in the range of 30-105 J/cm^2 was investigated by MTT assay. The mortality rate of MCF-7 and MDA-MB-231 cells treated with MTX- FA loaded Au@SiO_2 NPs (the MTX concentration was 100 μg/mL) after LLLT at a dose of 75 J/cm^2 were about 39 and 45.5%, respectively. While at the same condition the cells treated with Au@SiO_2 NPs after laser irradiation or laser alone did not show obvious cell death. Also by increasing the laser dose to 105 J/cm^2 the mortality rate of both cell lines increased to 60-75%, while both cell liness treated with Au@SiO_2 NPs +laser or laser alone at the same irradiation dose showed no cytotoxic effect. The IC50 value for MCF-7 and MDA-MB-231 cells after combination therapy with MTX-FA loaded Au@SiO_2 NPs (MTX dose of 100 μg/mL) and LLLT were obtained at a dose of 90 and 75 J/cm^2, respectively. On the other hand the mortality rate of MTX and MTX-FA loaded Au@SiO_2NPs without laser irradiation at MTX dose of 100 μg/mL (selected dose for laser therapy study) was between 15-25% in both cell lines. These results indicated that the combination of MTX-FA loaded Au@SiO_2NPs and laser therapy showed a synergistic effect in both cell lines and significantly decreased the

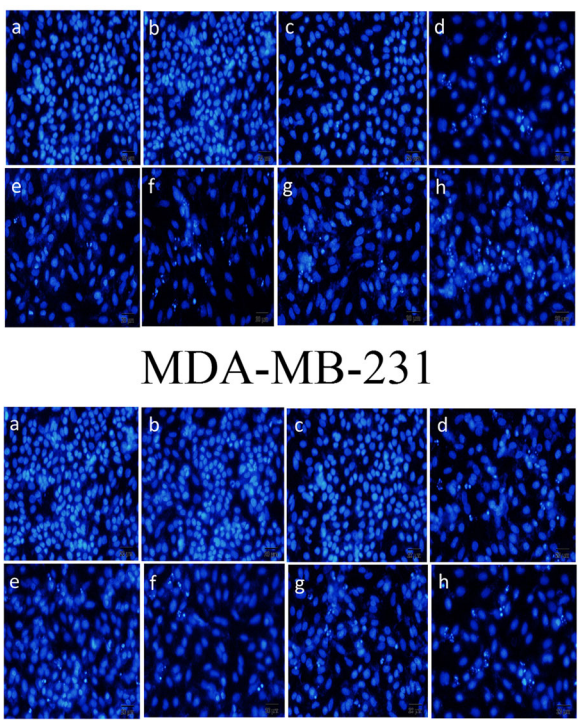

Fig. 8 Apoptosis assay using DAPI staining for MCF-7 or MDA-MB-231 cells, images captured using an inverted microscope. The untreated cells as the negative control (**a**), cells treated with laser (75 J/cm^2) as positive control (**b**) cells treated with Au@SiO_2 nanoparticles (NP (**c**), cells treated with laser (75 J/cm^2) and Au@SiO_2 nanoparticles (NP) (**d**), cells treated with MTX without laser irradiation (**e**), cells treated with MTX and laser irradiation (**f**), cells treated with MTX-FA-loaded Au@SiO_2 nanoparticles (NPD) without laser exposure (**g**), and cells treated with MTX-FA-loaded Au@SiO_2 nanoparticles (NPD) with Laser exposure (**h**)

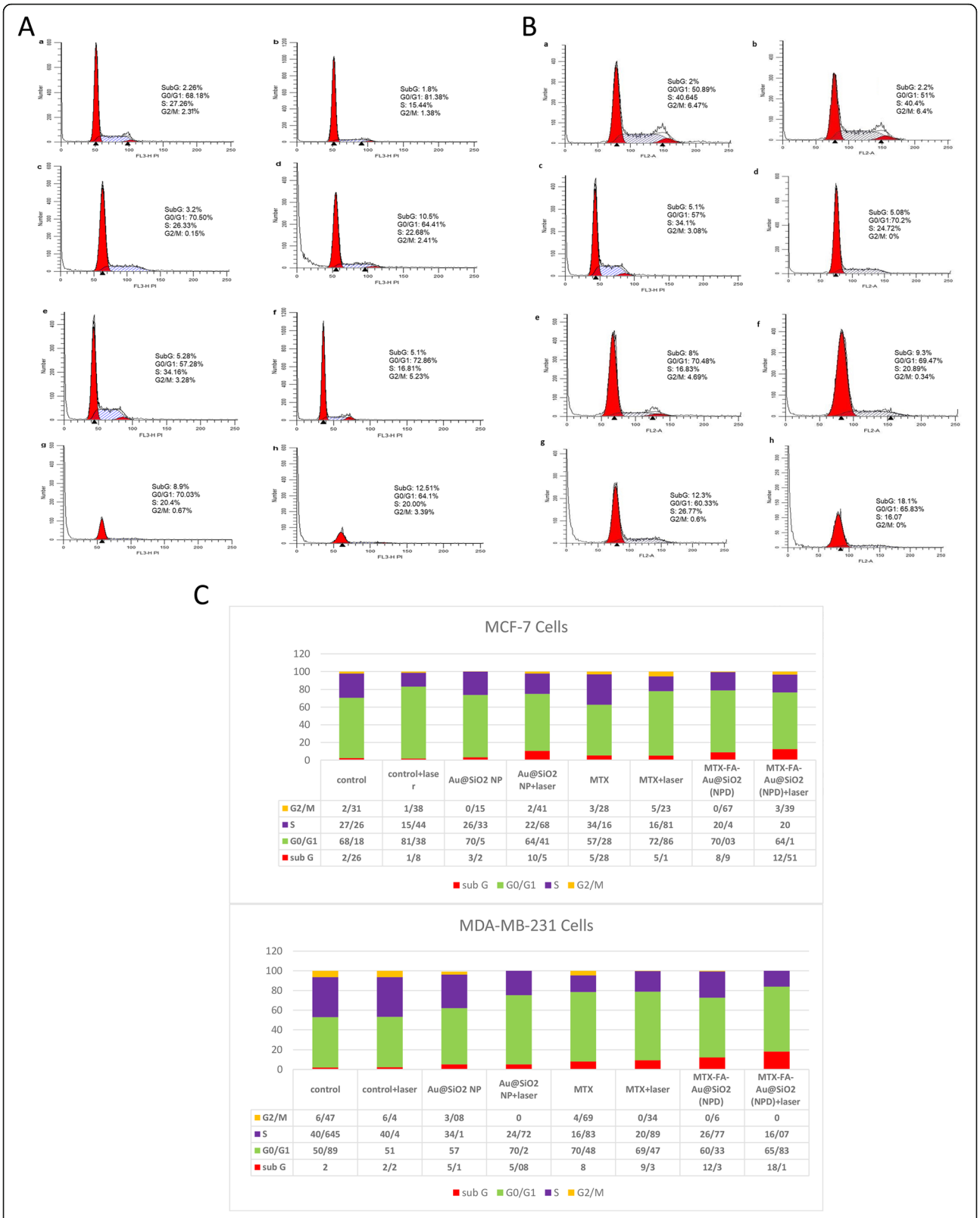

MCF-7 Cells	control	control+laser	Au@SiO2 NP	Au@SiO2 NP+laser	MTX	MTX+laser	MTX-FA-Au@SiO2 (NPD)	MTX-FA-Au@SiO2 (NPD)+laser
G2/M	2/31	1/38	0/15	2/41	3/28	5/23	0/67	3/39
S	27/26	15/44	26/33	22/68	34/16	16/81	20/4	20
G0/G1	68/18	81/38	70/5	64/41	57/28	72/86	70/03	64/1
sub G	2/26	1/8	3/2	10/5	5/28	5/1	8/9	12/51

MDA-MB-231 Cells	control	control+laser	Au@SiO2 NP	Au@SiO2 NP+laser	MTX	MTX+laser	MTX-FA-Au@SiO2 (NPD)	MTX-FA-Au@SiO2 (NPD)+laser
G2/M	6/47	6/4	3/08	0	4/69	0/34	0/6	0
S	40/645	40/4	34/1	24/72	16/83	20/89	26/77	16/07
G0/G1	50/89	51	57	70/2	70/48	69/47	60/33	65/83
sub G	2	2/2	5/1	5/08	8	9/3	12/3	18/1

Fig. 9 (See legend on next page.)

(See figure on previous page.)
Fig. 9 Cell cycle distributions investigated for MCF-7 (**A**) or MDA-MB-231 (**B**) cells. The untreated cells as negative control (**a**), cells treated with laser (75 J/cm^2) as positive control (**b**) cells treated with Au@SiO_2 nanoparticles (NP) (**c**), cells treated with laser (75 J/cm^2) and Au@SiO_2 nanoparticles (NP) (**d**), cells treated with MTX without laser irradiation (**e**), cells treated with MTX and laser irradiation (**f**), cells treated with MTX-FA-loaded Au@SiO_2 nanoparticles (NPD) without laser exposure (**g**), and cells treated with MTX-FA-loaded Au@SiO_2 nanoparticles (NPD) with Laser exposure (**h**), **C**) Quantitative results of cell cycle arrest and its distribution

cell viability (p<0.001) compared to cells received only laser irradiation. These results indicated that NPs treatment, especially with targeting strategy can improved the efficacy of laser therapy in breast cancer cell destruction (Fig. 7).

Apoptosis study by DAPI

The apoptosis were studied in MCF-7 and MDA-MB-231 cells after treatment with Au@ SiO_2 NPs; MTX-FA loaded Au@ SiO_2 NPs with or without laser to know if laser treatment could enhance the efficacy of chemotherapy. Our results summarized in Fig. 8 indicated that normal MCF-7 and MDA-MB-231 cells without any treatment set as control as well as cells treated with laser alone or free Au@SiO_2 NPs without laser irradiation had typical nuclei, lacking any apoptosis. However, MCF-7 and MDA-MB-231 cells treated with free MTX, Au@ SiO_2 NPs with laser irradiation and MTX and FA loaded Au@SiO_2 NPs without laser irradiation showed partial apoptotic nuclei (Fig. 8). The cells treated with MTX and FA loaded Au@SiO_2 NPs in combination with laser irradiation (810 nm, 75 J/cm^2, 139 sec) showed a major drop in MCF-7 and MDA-MB-231 cell population. Therefore, laser irradiation efficacy was enhanced after MTX/FA loaded Au@SiO_2 NPs uptake on MCF-7 and MDA-MB-231 cells. Hence, the novel developed MTX and FA loaded Au@SiO_2 NPs has the capability of augmenting the photothermal effects by highly fragmented cell nuclei, a radical rise in cell loss and complete damage of cells.

Cell cycle

Cell cycle distributions after treatment with MTX, Au@SiO_2 NPs and MTX and FA loaded Au@SiO_2 NPs either in combination with LLLT (75 J/cm^2) or without laser irradiation was studied in both MCF-7 and MDA-MB-231 cells using flowcytometry and PI staining of DNA. Our study indicated that in MDA-MB-231 or MCF-7 cells, the percentage of non-treated cells (control group) were actively in phase S (Fig. 9a, b). Using 75 J/cm^2 laser treatments reduced the percentage of cells in S-phase in a non-significant manner. On the other hand the cells irradiated with LLLT without NP and drug treatment showed the significant increase in Go/G1 cell population indicated the safety of LLLT alone. Also NPs treatment did not disturb the cell cycle in both cell lines. Treatment of cells with free MTX in the absence or presence of laser irradiation showed some disturbances in cell cycles, including reduction of cells in S-phase. Using NPD alone reduced the cells in S-phase. And interestingly using MTX and FA loaded Au@SiO_2 NPs (NPD) enhanced the cell percentage in sub Go/G1 as a sign of apoptosis [72]. Also the percentage of the MDA-MB-231 cells present in sub Go/G1 (around 18%) were significantly higher than MCF-7 cells (12%) in MTX and FA loaded Au@SiO_2 NPs (NPD) treatment group due to the higher uptake of NPs in MDA-MB-231 cells.

Ramos *et al*, showed that in tumor cells, LLLT increases the percentage of cells in S and G2 /M phases, also they detected a reduction in proliferation and enhancing in senescence [79]. The cell cycle study after LLLT (15 J/cm2) showed a G1 arrest, which is in line with growth stopover in irradiated TK6 cells [80]. Another group reported that PTT is primarily disturbing cells in the S phase and increasing the cell population and arrest in the G2/M phase [81]. As a result, PTT can induce radio-sensitization of the cells via disturbing cell cycle [82]. Their results are in accordance with our study, which showed cell cycle disturbance and reduction of cells in S-phase. Our study also showed the increase in population of apoptotic cells (sub Go/G1) after combination chemo-photothermal therapy. Therefore, applying a combination of LLLT and MTX and FA loaded Au@SiO_2 NPs (NPD) as breast cancer targeted nanoparticles could enhance the breast cancer therapy efficacy.

Conclusions

In this study MTX and FA loaded Au@SiO_2 NPs was designed for target breast cancer therapy in combination with LLLT as noninvasive, FDA approved laser therapy. MTX and FA loaded Au@SiO_2 NPs with spherical morphology and mean diameter of 25nm and surface charge of -19.7 was obtained. This size and surface charge is in a suitable range to increase the biodistribution of NPs. The successful targeted strategy of this novel developed NPs was approved with a higher cellular uptake percentage of MDA-MB-231 compared to MCF-7 as two breast cancer cell lines with different folate receptor expression. The MTT assay, DAPI staining and cell cycle study's results indicated that the combination of chemo-photothermal therapy showed synergistic effect and the cytotoxicity and apoptosis effect on both breast cancer cell lines especially on MDA-MB-231 cells was increased significantly(p<0.001).

Since the $Au@SiO_2$ nanoparticles or LLLT showed no cytotoxic effects, it can be concluded that our therapeutic design has synergistic effects on targeted site. The findings of this study could be useful for designing future cancer therapy programs using bio-chemotherapy combined with low level lasers.

Abbreviations

$Au@SiO_2$: Silica coated gold; BC: Breast cancer; DHFR: Dihydrofolate reductase; DMSO: Dimethyl Sulfoxide; FA: Folate; LLLT: Low level laser therapy; LSPR: Localized surface plasmon resonance; MSN: Mesoporous silica nanoparticle; MTX: Methotrexate; NIR: Near-infrared; NPs: Nanoparticles; PTT: Photothermal therapy; RhoD: rhodamine B; TFSNPs: Thiol-functionalized silica-coated nanoparticles

Acknowledgements

Not applicable

Authors' Contributions

RA: data collection and figure preparation. SHR: Contributed in all laser experiments. MRY: Advice on conducting cell based tests. RS and EA: equally contributed in conceptualization and contributed to the organization, writing and edition of manuscript. All authors read and approved the final manuscript.

Funding

This project was supported financially by Research Vice Chancellor, Faculty of advanced Medical Sciences, Tabriz University of Medical Sciences, and grant number: 95/2-2/2.

Availability of Data and Materials

Not applicable

Competing Interests

The authors declare that they have no competing interests.

Author details

[1]Department of Medical Biotechnology, Faculty of Advanced Medical Sciences, Tabriz University of Medical Sciences, Tabriz, Iran. [2]Department of Medical Bioengineering, Tabriz University of Medical Sciences, Tabriz, Iran. [3]Drug Applied Research Center and Department of Medical Nanotechnology, Faculty of Advanced Medical Sciences, Tabriz University of Medical Sciences, Tabriz, Iran.

Received: 27 May 2019 Accepted: 5 March 2020
Published online: 19 March 2020

References

1. Ferlay J, Soerjomataram I, Dikshit R, Eser S, Mathers C, Rebelo M et al (2015) Cancer incidence and mortality worldwide: sources, methods and major patterns in GLOBOCAN 2012. Int J Cancer 136(5):E359–EE86
2. Aghaee F, Pirayesh Islamian J, Baradaran B (2012) Enhanced radiosensitivity and chemosensitivity of breast cancer cells by 2-deoxy-d-glucose in combination therapy. J Breast Cancer 15(2):141–147
3. Dias MF, Sousa E, Cabrita S, Patrício J, Oliveira CF (2000) Chemoprevention of DMBA-induced mammary tumors in rats by a combined regimen of alpha-tocopherol, selenium, and ascorbic acid. Breast J 6(1):14–19
4. Parkin DM, Bray F, Ferlay J, Pisani P (2005) Global cancer statistics, 2002. CA Cancer J Clin 55(2):74–108
5. Movahedi M, Haghighat S, Khayamzadeh M, Moradi A, Ghanbari-Motlagh A, Mirzaei H et al (2012) Survival rate of breast cancer based on geographical variation in Iran, a national study. Iran Red Crescent Med J 14(12):798
6. McPherson K, Steel C, Dixon J (2000) ABC of breast diseases: breast cancer—epidemiology, risk factors, and genetics. BMJ 321(7261):624
7. De La Rochefordiere A, Campana F, Fenton J, Vilcoq J, Fourquet A, Asselain B et al (1993) Age as prognostic factor in premenopausal breast carcinoma. Lancet. 341(8852):1039–1043
8. Leong SP, Shen Z-Z, Liu T-J, Agarwal G, Tajima T, Paik N-S et al (2010) Is breast cancer the same disease in Asian and Western countries? World J Surg 34(10):2308–2324
9. Cancer CGoHFiB (2012) Menarche, menopause, and breast cancer risk: individual participant meta-analysis, including 118 964 women with breast cancer from 117 epidemiological studies. Lancet Oncol 13(11):1141–1151
10. Buchholz TA, Hill B, Tucker S, Frye D, Kuerer HM, Buzdar A et al (2001) Factors predictive of outcome in patients with breast cancer refractory to neoadjuvant chemotherapy. Cancer J (Sudbury, Mass) 7(5):413–420
11. Romond EH, Perez EA, Bryant J, Suman VJ, Geyer CE Jr, Davidson NE et al (2005) Trastuzumab plus adjuvant chemotherapy for operable HER2-positive breast cancer. N Engl J Med 353(16):1673–1684
12. Smith I, Procter M, Gelber RD, Guillaume S, Feyereislova A, Dowsett M et al (2007) 2-year follow-up of trastuzumab after adjuvant chemotherapy in HER2-positive breast cancer: a randomised controlled trial. Lancet 369(9555):29–36
13. Hamdy S, Haddadi A, Hung RW, Lavasanifar A (2011) Targeting dendritic cells with nano-particulate PLGA cancer vaccine formulations. Adv Drug Deliv Rev 63(10-11):943–955
14. Sheng W-Y, Huang L (2011) Cancer immunotherapy and nanomedicine. Pharm Res 28(2):200–214
15. Neidle S, Thurston DE (2005) Chemical approaches to the discovery and development of cancer therapies. Nat Rev Cancer 5(4):285
16. Davis ME, Chen Z, Shin DM (2010) Nanoparticle therapeutics: an emerging treatment modality for cancer. Nanosci Technol:239–250
17. Chu KF, Dupuy DE (2014) Thermal ablation of tumours: biological mechanisms and advances in therapy. Nat Rev Cancer 14(3):199
18. Chen Z, Wang Q, Wang H, Zhang L, Song G, Song L et al (2013) Ultrathin PEGylated W18O49 Nanowires as a New 980 nm-Laser-Driven Photothermal Agent for Efficient Ablation of Cancer Cells In Vivo. Adv Mater 25(14):2095–2100
19. Yang K, Yang G, Chen L, Cheng L, Wang L, Ge C et al (2015) FeS nanoplates as a multifunctional nano-theranostic for magnetic resonance imaging guided photothermal therapy. Biomaterials. 38:1–9
20. Moon HK, Lee SH, Choi HC (2009) In vivo near-infrared mediated tumor destruction by photothermal effect of carbon nanotubes. ACS Nano 3(11):3707–3713
21. Yu J, Javier D, Yaseen MA, Nitin N, Richards-Kortum R, Anvari B et al (2010) Self-assembly synthesis, tumor cell targeting, and photothermal capabilities of antibody-coated indocyanine green nanocapsules. J Am Chem Soc 132(6):1929–1938
22. Jaque D, Maestro LM, Del Rosal B, Haro-Gonzalez P, Benayas A, Plaza J et al (2014) Nanoparticles for photothermal therapies. Nanoscale 6(16):9494–9530
23. Yang K, Zhang S, Zhang G, Sun X, Lee S-T, Liu Z (2010) Graphene in mice: ultrahigh in vivo tumor uptake and efficient photothermal therapy. Nano Lett 10(9):3318–3323
24. Yuan H, Fales AM, Vo-Dinh T (2012) TAT peptide-functionalized gold nanostars: enhanced intracellular delivery and efficient NIR photothermal therapy using ultralow irradiance. J Am Chem Soc 134(28):11358–11361
25. Tian Q, Hu J, Zhu Y, Zou R, Chen Z, Yang S et al (2013) Sub-10 nm Fe3O4@Cu2–x S Core–Shell Nanoparticles for Dual-Modal Imaging and Photothermal Therapy. J Am Chem Soc 135(23):8571–8577
26. Zha Z, Wang S, Zhang S, Qu E, Ke H, Wang J et al (2013) Targeted delivery of CuS nanoparticles through ultrasound image-guided microbubble destruction for efficient photothermal therapy. Nanoscale. 5(8):3216–3219
27. Han J, Li J, Jia W, Yao L, Li X, Jiang L et al (2014) Photothermal therapy of cancer cells using novel hollow gold nanoflowers. Int J Nanomedicine 9:517
28. Geng J, Sun C, Liu J, Liao LD, Yuan Y, Thakor N et al (2015) Biocompatible conjugated polymer nanoparticles for efficient photothermal tumor therapy. Small. 11(13):1603–1610
29. Agarwal A, Mackey MA, El-Sayed MA, Bellamkonda RV (2011) Remote triggered release of doxorubicin in tumors by synergistic application of thermosensitive liposomes and gold nanorods. ACS Nano 5(6):4919–4926
30. Dreaden EC, El-Sayed MA (2012) Detecting and destroying cancer cells in more than one way with noble metals and different confinement properties on the nanoscale. Acc Chem Res 45(11):1854–1865
31. Farokhzad OC, Langer R (2009) Impact of nanotechnology on drug delivery. ACS Nano 3(1):16–20
32. Ferrari M (2005) Cancer nanotechnology: opportunities and challenges. Nat Rev Cancer 5(3):161
33. Koo OM, Rubinstein I, Onyuksel H (2005) Role of nanotechnology in targeted drug delivery and imaging: a concise review. Nanomedicine 1(3):193–212
34. Nishiyama N (2007) Nanomedicine: nanocarriers shape up for long life. Nat Nanotechnol 2(4):203

35. Peer D, Karp JM, Hong S, Farokhzad OC, Margalit R, Langer R (2007) Nanocarriers as an emerging platform for cancer therapy. Nat Nanotechnol 2(12):751
36. Hirsch LR, Stafford RJ, Bankson J, Sershen SR, Rivera B, Price R et al (2003) Nanoshell-mediated near-infrared thermal therapy of tumors under magnetic resonance guidance. Proc Natl Acad Sci 100(23):13549–13554
37. Zharov VP, Galitovsky V, Viegas M (2003) Photothermal detection of local thermal effects during selective nanophotothermolysis. Appl Phys Lett 83(24):4897–4899
38. Zharov VP, Kim J-W, Curiel DT, Everts M (2005) Self-assembling nanoclusters in living systems: application for integrated photothermal nanodiagnostics and nanotherapy. Nanomedicine 1(4):326–345
39. Chakravarty P, Qian W, El-Sayed MA, Prausnitz MR (2010) Delivery of molecules into cells using carbon nanoparticles activated by femtosecond laser pulses. Nat Nanotechnol 5(8):607
40. Banu H, Sethi DK, Edgar A, Sheriff A, Rayees N, Renuka N et al (2015) Doxorubicin loaded polymeric gold nanoparticles targeted to human folate receptor upon laser photothermal therapy potentiates chemotherapy in breast cancer cell lines. J Photochem Photobiol B 149:116–128
41. Nikoobakht B, El-Sayed MA (2003) Preparation and growth mechanism of gold nanorods (NRs) using seed-mediated growth method. Chem Mater 15(10):1957–1962
42. Huang X, El-Sayed IH, Qian W, El-Sayed MA (2006) Cancer cell imaging and photothermal therapy in the near-infrared region by using gold nanorods. J Am Chem Soc 128(6):2115–2120
43. Guerrero AR, Hassan N, Escobar CA, Albericio F, Kogan MJ, Araya E (2014) Gold nanoparticles for photothermally controlled drug release. Nanomedicine. 9(13):2023–2039
44. Connor EE, Mwamuka J, Gole A, Murphy CJ, Wyatt MD (2005) Gold nanoparticles are taken up by human cells but do not cause acute cytotoxicity. Small. 1(3):325–327
45. Xiao Y, Hong H, Matson VZ, Javadi A, Xu W, Yang Y et al (2012) Gold nanorods conjugated with doxorubicin and cRGD for combined anticancer drug delivery and PET imaging. Theranostics. 2(8):757
46. Wu C, Yu C, Chu M (2011) A gold nanoshell with a silica inner shell synthesized using liposome templates for doxorubicin loading and near-infrared photothermal therapy. Int J Nanomedicine 6:807
47. Liu Y, Xu M, Chen Q, Guan G, Hu W, Zhao X et al (2015) Gold nanorods/mesoporous silica-based nanocomposite as theranostic agents for targeting near-infrared imaging and photothermal therapy induced with laser. Int J Nanomedicine 10:4747
48. Cho K, Wang X, Nie S, Shin DM (2008) Therapeutic nanoparticles for drug delivery in cancer. Clin Cancer Res 14(5):1310–1316
49. Cai W, Gao T, Hong H, Sun J (2008) Applications of gold nanoparticles in cancer nanotechnology. Nanotechnol Sci Appl 1:17
50. Palmer BV, Walsh G, McKinna J, Greening W (1980) Adjuvant chemotherapy for breast cancer: side effects and quality of life. Br Med J 281(6255):1594–1597
51. Greene D, Nail L, Fieler V, Dudgeon D, Jones L (1994) A comparison of patient-reported side effects among three chemotherapy regimens for breast cancer. Cancer Pract 2(1):57–62
52. Beisecker AE, Cook MR, Ashworth J, Hayes J, Brecheisen M, Helmig L et al (1997) Side effects of adjuvant chemotherapy: perceptions of node-negative breast cancer patients. Psycho-Oncol 6(2):85–93
53. Reichman BS, Green KB (1994) Breast cancer in young women: effect of chemotherapy on ovarian function, fertility, and birth defects. J Natl Cancer Institute Monographs 16:125–129
54. Furst D (1985) Clinical pharmacology of very low dose methotrexate for use in rheumatoid arthritis. J Rheumatol Supplement 12:11–14
55. Jolivet J, Cowan KH, Curt GA, Clendeninn NJ, Chabner BA (1983) The pharmacology and clinical use of methotrexate. N Engl J Med 309(18):1094–1104
56. Schweitzer BI, Dicker AP, Bertino JR (1990) Dihydrofolate reductase as a therapeutic target. FASEB J 4(8):2441–2452
57. Meng F, Hennink WE, Zhong Z (2009) Reduction-sensitive polymers and bioconjugates for biomedical applications. Biomaterials. 30(12):2180–2198
58. Bae Y, Fukushima S, Harada A, Kataoka K (2003) Design of environment-sensitive supramolecular assemblies for intracellular drug delivery: Polymeric micelles that are responsive to intracellular pH change. Angew Chem 115(38):4788–4791
59. Shen J, He Q, Gao Y, Shi J, Li Y (2011) Mesoporous silica nanoparticles loading doxorubicin reverse multidrug resistance: performance and mechanism. Nanoscale. 3(10):4314–4322
60. Campbell IG, Jones TA, Foulkes WD, Trowsdale J (1991) Folate-binding protein is a marker for ovarian cancer. Cancer Res 51(19):5329–5338
61. Sabharanjak S, Mayor S (2004) Folate receptor endocytosis and trafficking. Adv Drug Deliv Rev 56(8):1099–1109
62. Rasouli S, Davaran S, Rasouli F, Mahkam M, Salehi R (2014) Positively charged functionalized silica nanoparticles as nontoxic carriers for triggered anticancer drug release. Designed Monomers Polymers 17(3):227–237
63. Salehi R, Alizadeh E, Kafil HS, Hassanzadeh AM, Mahkam M (2015) pH-Controlled multiple-drug delivery by a novel antibacterial nanocomposite for combination therapy. RSC Adv 5(128):105678–105691
64. Darfarin G, Salehi R, Alizadeh E, Nasiri Motlagh B, Akbarzadeh A, Farajollahi A (2018) The effect of SiO2/Au core–shell nanoparticles on breast cancer cell's radiotherapy. Artificial Cells Nanomed Biotechnol:1–11
65. Gharatape A, Milani M, Rasta SH, Pourhassan-Moghaddam M, Ahmadi-Kandjani S, Davaran S et al (2016) A novel strategy for low level laser-induced plasmonic photothermal therapy: the efficient bactericidal effect of biocompatible AuNPs@(PNIPAAM-co-PDMAEMA, PLGA and chitosan). RSC Adv 6(112):110499–110510
66. Davaran S, Fazeli H, Ghamkhari A, Rahimi F, Molavi O, Anzabi M et al (2018) Synthesis and Characterization of Novel P (HEMA-LA-MADQUAT) micelles for co-delivery of Methotrexate and Chrysin in combination cancer chemotherapy. J Biomat Sci Polymer Edition 29(11):1265–1286
67. Meier R, Henning TD, Boddington S, Tavri S, Arora S, Piontek G et al (2010) Breast cancers: MR imaging of folate-receptor expression with the folate-specific nanoparticle P1133. Radiology. 255(2):527–535
68. Mousazadeh L, Alizadeh E, Zarghami N, Hashemzadeh S, Aval SF, Hasanifard L, et al. Histone Deacetylase Inhibitor (Trapoxin A) Enhances Stemness Properties in Adipose Tissue Derived Mesenchymal Stem Cells. Drug Res (Stuttg). (EFirst).
69. Honary S, Zahir F (2013) Effect of zeta potential on the properties of nano-drug delivery systems-a review (Part 1). Trop J Pharm Res 12(2):255–264
70. Gustafson HH, Holt-Casper D, Grainger DW, Ghandehari H (2015) Nanoparticle uptake: the phagocyte problem. Nano Today 10(4):487–510
71. Oh N, Park J-H (2014) Endocytosis and exocytosis of nanoparticles in mammalian cells. Int J Nanomedicine 9(Suppl 1):51
72. Rahimi M, Safa KD, Alizadeh E, Salehi R (2017) Dendritic chitosan as a magnetic and biocompatible nanocarrier for the simultaneous delivery of doxorubicin and methotrexate to MCF-7 cell line. New J Chem 41(8):3177–3189
73. Parker N, Turk MJ, Westrick E, Lewis JD, Low PS, Leamon CP (2005) Folate receptor expression in carcinomas and normal tissues determined by a quantitative radioligand binding assay. Anal Biochem 338(2):284–293
74. Tian D-Y, Wang W-Y, Li S-P, Li X-D, Sha Z-L (2016) A novel platform designed by Au core/inorganic shell structure conjugated onto MTX/LDH for chemo-photothermal therapy. Int J Pharm 505(1-2):96–106
75. Wang S, Li K, Chen Y, Chen H, Ma M, Feng J et al (2015) Biocompatible PEGylated MoS2 nanosheets: Controllable bottom-up synthesis and highly efficient photothermal regression of tumor. Biomaterials. 39:206–217
76. Patel K, Raj BS, Chen Y, Lou X (2016) Cytotoxicity of folic acid conjugated hollow silica nanoparticles toward Caco2 and 3T3 cells, with and without encapsulated DOX. Colloids Surf B: Biointerfaces 140:213–222
77. Yao Y, Shi X, Chen F (2014) The effect of gold nanoparticles on the proliferation and differentiation of murine osteoblast: a study of MC3T3-E1 cells in vitro. J Nanosci Nanotechnol 14:4851–4857
78. Li C, Li Z, Wang Y, Liu H (2016) Gold Nanoparticles Promote Proliferation of Human Periodontal Ligament Stem Cells and Have Limited Effects on Cells Differentiation. J Nanomater 10
79. Ramos Silva C, Cabral FV, de Camargo CFM, Núñez SC, Mateus Yoshimura T, de Lima Luna AC et al (2016) Exploring the effects of low-level laser therapy on fibroblasts and tumor cells following gamma radiation exposure. J Biophotonics 9(11-12):1157–1166
80. Mognato M, Squizzato F, Facchin F, Zaghetto L, Corti L (2004) Cell growth modulation of human cells irradiated in vitro with low-level laser therapy. Photomed Laser Surg 22(6):523–526
81. Li P, Shi YW, Li BX, Xu WC, Shi ZL, Zhou C et al (2015) Photo-thermal effect enhances the efficiency of radiotherapy using Arg-Gly-Asp peptides-conjugated gold nanorods that target alphavbeta3 in melanoma cancer cells. J Nanobiotechnol 13:52
82. Norouzi H, Khoshgard K, Akbarzadeh F (2018) In vitro outlook of gold nanoparticles in photo-thermal therapy: a literature review. Lasers Med Sci:1–10

Publisher's Note